# Magnetoreflectivity of $Pb_{1-x}Eu_xTe$ epilayers and $PbTe/Pb_{1-x}Eu_xTe$ multiple quantum wells

Shu Yuan,* Heinz Krenn, Gunther Springholz, Yukio Ueta, and Günther Bauer
*Institut für Halbleiterphysik, Johannes Kepler Universität, A-4040 Linz, Austria*

Patrick J. McCann
*School of Electrical Engineering, University of Oklahoma, Norman, Oklahoma 73019*
(Received 30 May 1996)

Molecular-beam epitaxy grown *n*-type $Pb_{1-x}Eu_xTe$ epilayers ($x \leqslant 0.034$) and $PbTe/Pb_{1-x}Eu_xTe$ ($x \leqslant 0.039$) multiple-quantum-well (MQW) samples were studied by magnetoreflectivity in the Faraday configuration ($B \| [111]$) for magnetic fields up to 6 T at 4.2 K. Since the IV-VI lead salt compounds are quite polar semiconductors, resonant electron-longitudinal-optic- (LO-) phonon coupling (Fröhlich coupling) modifies the cyclotron resonance (CR) energies in the $Pb_{1-x}Eu_xTe$ single epilayers for the three-dimensional (3D) case. Due to the many-valley band structure *two* different Fröhlich coupling constants are relevant. However, the CR energies of quasi-two-dimensional (2D) carriers in PbTe wells [$n^{2D}=(1.5-3)\times 10^{11}$ cm$^{-2}$] of $PbTe/Pb_{1-x}Eu_xTe$ MQW samples do *not* exhibit a significant resonant electron-LO-phonon interaction. This observation is attributed to finite-electron concentration effects, in particular, to a partial filling of the lowest 2D Landau spin level. The static and dynamic screening of the polar interaction are considered as well, but are ruled out as an explanation for the absence of any remarkable polaron correction to the CR energies of electrons in the PbTe quantum wells for the range of carrier concentrations investigated. The magnetoreflectivity spectra of $Pb_{1-x}Eu_xTe$ single layers and $PbTe/Pb_{1-x}Eu_xTe$ quantum well samples are simulated numerically, using a model for the dielectric response of IV-VI compounds in a magnetic field, which also includes the electron-LO-phonon interaction. The transverse and longitudinal masses, and thus also the interband momentum matrix elements are determined for $Pb_{1-x}Eu_xTe$ as a function of the composition up to $x<0.034$. It is found that the transverse mass *increases* with Eu content, whereas the longitudinal one nearly stays constant. The 2D CR masses of electrons in the PbTe wells increase with decreasing well width, i.e., with increasing quantum-well interband energies, a behavior which results from the strong band nonparabolicity. [S0163-1829(97)03807-1]

## I. INTRODUCTION

IV-VI compound semiconductors and their quantum-well (QW) structures have been used for quite a period of time for midinfrared detectors and laser diodes.[1–4] In particular, the fabrication of *p-n* junction laser diodes has benefitted from the molecular-beam epitaxial (MBE) growth of binary, ternary, and quaternary compounds based on PbSe and PbTe.[1] Multiple-element infrared focal-plane photodetector arrays have been fabricated using IV-VI epilayers grown on Si substrates with sensitivities not much inferior to $Hg_{1-x}Cd_xTe$, but with much less demanding material processing steps.[5] Recently, there has been further progress in the MBE growth of IV-VI compounds[6] and, e.g., for $PbTe/Pb_{1-x}Eu_xTe$ quantum-well samples grown on (111) $BaF_2$ substrates the observation of the quantum Hall effect has been reported.[7,8] Also the successful growth of IV-VI compounds lattice matched to (100) $BaF_2$ substrates has been reported recently.[9]

The progress which has been achieved in the MBE growth of the lead salt compounds and which has made possible these applications as midinfrared lasers and advanced detectors also yields bulklike and quantum-well samples with which some basic phenomena can be studied. The lead salt compounds are quite polar semiconductors with a Fröhlich coupling constant $\alpha$ of the order of 0.2. Thus the cyclotron resonance of electrons and holes should exhibit a modification of the Landau levels due to polaron coupling whenever the cyclotron frequency $\hbar\omega_c$ becomes comparable to the longitudinal-optic-phonon frequency $\hbar\omega_{\mathrm{LO}}$.[10–13] For $\alpha=0.2$, the weak-coupling limit is still applicable.[10] Polaron coupling phenomena have been observed in the past in PbTe, but a quantitative description of the carrier-LO-phonon interaction in this many valley semiconductor is still not yet available. In addition to studies of the polaron interaction in three-dimensional (3D) systems, it is well known that polaron effects have to be considered for the interpretation of the cyclotron resonance energies in two-dimensional (2D) systems, like carriers confined at heterojunctions or in narrow quantum wells.[13] However, in 2D systems with a relatively high electron density the polaron enhancement of the cyclotron mass may be in competition with many-body screening effects of the electron-polar-phonon interaction. In addition, it is well known that Landau-level occupation effects have a drastic influence on the resonant magnetopolaron interaction.[14–16]

In this paper we address the problem of the electron-LO-phonon interaction in epilayers of $Pb_{1-x}Eu_xTe$ with Eu contents ranging from 0 to about 3.43%. These epilayers are several $\mu$m thick and thus even at $T=4.2$ K the carriers behave 3D-like. Because of the peculiarities of the polar-phonon contribution to the total frequency-dependent dielectric function in these materials with a huge difference of the static ($\varepsilon_0 \approx 1400$ at $T=4.2$ K) and high-frequency dielectric

 

TABLE I. Sample parameters for $Pb_{1-x}Eu_xTe$ single layers. Eu content $x$, energy gap $E_g$ at 4.2 K, epilayer thickness $d$, electron concentration $n$, and electron mobilities $\mu$ are given.

| Sample No. | $x$ (%) | $E_g$ (meV) | $d$ ($\mu$m) | $n$ ($10^{16}$ cm$^{-3}$) | $\mu$ ($10^3$ cm$^2$/V s) |
|---|---|---|---|---|---|
| No. 127 | 0 | 189.7 | 4.5 | 3.2 | 465 (20 K) |
| No. 143 | 1.30 | 248 | 4.9 | 40 | 50 (4.2 K) |
| No. 199 | 1.73 | 267 | 3.9 | 2.5 | 100 (4.2 K) |
| No. 114 | 2.45 | 299 | 4.3 | 2.2 | 3.1 (77 K) |
| No. 145 | 3.43 | 343 | 4.2 | 5.0 | 20 (4.2 K) |

constant ($\varepsilon_\infty \approx 36$) we have used far-infrared magnetoreflectivity studies in Faraday configuration with the magnetic-field $B$ oriented parallel to the [111] growth direction, to get information on the cyclotron resonance energies as a function of the magnetic field. From the cyclotron resonance frequencies in these many valley semiconductors, the dependence of the transverse and longitudinal electron effective masses on the Eu content is obtained. Furthermore pinning phenomena are observed when the cyclotron resonance frequency $\hbar\omega_c$ becomes comparable to the longitudinal-optic-phonon frequency $\hbar\omega_{\mathrm{LO}}$ both for the carriers in the longitudinal ([111]) and the three oblique ($\langle 111\rangle$) valleys. The $n=1$ Landau level becomes double valued for magnetic fields corresponding to $\hbar\omega_c \geqslant \hbar\omega_{\mathrm{LO}}$. A splitting of cyclotron resonance absorption and a corresponding polaron-induced change of the effective mass can be observed for this regime of magnetic fields.[12,17]

The electron-polar optical-phonon interaction for many-valley semiconductors has been treated by Pekar and co-workers[18,19] and Larsen[20] in a series of papers. For PbTe electrons and holes are located in valleys at the $L$ point of the Brillouin zone, with a mass anisotropy ratio of about 10, but interact with LO phonons at the center of the Brillouin zone ($\hbar\omega_{\mathrm{LO}} \approx 14$ meV).

The knowledge and understanding of the 2D polaron effect at heterointerfaces between a wide- and narrow-gap semiconductor is still somewhat less developed than for the homogeneous 3D case. A large amount of experimental,[17,21–29] and theoretical work[13–16,30–32] has been devoted in the past to resonant polaron phenomena in 2D systems, mainly in III-V compounds. In contrast to the theoretical predictions for much larger polaron mass renormalizations in 2D systems as compared to 3D ones, experimental findings usually indicated much smaller ones than expected.[21–25] According to Peeters *et al.*,[31] three corrections have to be considered for a description of the measurements in 2D structures:

(i) The nonzero width of the 2D electron channel reduces the electron-polar-phonon interaction considerably, since the polaron diameter is comparable to the confinement length.

(ii) The one-phonon polaron theories have to be corrected for Pauli's exclusion principle as accounted for by the Fermi-Dirac statistics. The finite Landau-level occupancy leads to a cyclotron resonance mass renormalization which is an oscillating function of the filling factor. Furthermore, even in materials like GaAs, the band nonparabolicity constitutes a competing effect which can be larger than the oscillatory contribution from the polaron effects.

(iii) The static or dynamic screening of the electron-phonon interaction by the presence of many electrons has to be taken into account.

In our experiments, polaron effects were observed for the 3D carriers in the semimagnetic $Pb_{1-x}Eu_xTe$ epilayers. However, in $PbTe/Pb_{1-x}Eu_xTe$ QW's, where the electron density in the PbTe QW's is of the order of $(1.5–3)\times 10^{11}$ cm$^{-2}$, essentially no resonant polaron interaction was observed.

To understand the experimental results, we develop a model for the simulation of the measured magnetoreflectivity spectra. By comparing the calculated and experimental spectra, we determine the effective masses by investigating the CR of carriers in the valleys oriented parallel and oblique to the [111] growth direction.

This paper is organized as follows: in Sec. II, we describe samples and experiments; in Sec. III, we outline the theoretical background used to simulate the experimental spectra; in Sec. IV we present the results, and in Secs. V and VI we discuss and summarize this work.

## II. SAMPLES AND EXPERIMENTS

The $Pb_{1-x}Eu_xTe$-samples were grown on cleaved (111) $BaF_2$ by MBE under ultrahigh-vacuum conditions. The beam flux rates from the PbTe-, Eu-, and $Te_2$-effusion cells were measured by an ion gauge beam flux monitor calibrated with a quartz-crystal thickness monitor for an absolute flux rate

TABLE II. Sample parameters for $PbTe/Pb_{1-x}Eu_xTe$ MQW samples. Layer thicknesses $d$, number of periods, Eu content $x$, lowest interband transition in PbTe QW's $E_{11}$ at 4.2 K, and energy gap of the $Pb_{1-x}Eu_xTe$ barriers and buffer layers at 4.2 K are given.

| Sample No. | $d$ (buffer) $\mu$m | $d$ (barrier) Å | $d$ (well) Å | No. of periods | $x$ (%) | $E_{11}$ (meV) | $E_g$ (barrier) (meV) |
|---|---|---|---|---|---|---|---|
| No. 157 | 4.6 | 486 | 118 | 30 | 3.23 | 203 | 334 |
| No. 156 | 5.0 | 641 | 91 | 39 | 3.36 | 210 | 340 |
| No. 151 | 5.2 | 621 | 62 | 46 | 3.50 | 224 | 346 |
| No. 148 | 4.9 | 648 | 93 | 50 | 3.85 | 210 | 362 |

measurement. *In situ* reflection high-energy electron diffraction (RHEED) at 35 keV was used to monitor the growth process. For low substrate temperatures a large number of RHEED intensity oscillations was observed for the PbTe and $Pb_{1-x}Eu_xTe$ growth,[33] which in turn could be used to determine the absolute growth rates, which in all cases was close to $1\mu$m/h. Detailed growth conditions are described elsewhere.[34] For all the MQW samples, the $Pb_{1-x}Eu_xTe$ buffer layer incorporates the same Eu-content $x$ as the $Pb_{1-x}Eu_xTe$ barrier layers within the $PbTe/Pb_{1-x}Eu_xTe$ MQW structures. The optical and electronic quality of the samples was examined by transmission and reflectivity measurements using Fourier-transform infrared (FTIR) spectroscopy[35–37] and is best reflected by quantum Hall effect (QHE) measurements.[7,8] FTIR transmission measurements at temperatures from 4.2 K to 300 K show Fabry-Perot (FP) oscillations (due to thickness fringes). The transmission at FP peaks is as high as 98% which indicates a very high finesse of the samples. The optical constants—absorption coefficient and refractive index—of the samples were determined from a numerical fit to the transmission spectra and interrelating them by a Kramers-Kronig transformation. Mid-infrared transmission measurements at different spots over the sample's surface, using an infrared microscope, reveal a high epilayer uniformity ($\sim 5\%$). FTIR photoconductivity (PC) measurements were performed as well.[36] PC signals were usually obtained at temperatures up to 240 K, which also indicates the high electronic quality of these samples, in accordance with mobility measurements.[38] The energy gaps of bulklike $Pb_{1-x}Eu_xTe$ layers and the QW interband transition energy of $PbTe/Pb_{1-x}Eu_xTe$-MQW's were determined both by FTIR transmission and photoconductivity measurements. The structural and geometrical parameters of the samples were determined by high-resolution x-ray diffraction.[39] They are summarized in Table I for $Pb_{1-x}Eu_xTe$ epilayers and in Table II for $PbTe/Pb_{1-x}Eu_xTe$ MQW samples, together with electrical transport parameters.

Magnetoreflectivity measurements were performed with a Bruker 113 v FTIR spectrometer to which a split-coil superconducting magnet with a low-temperature insert for optical measurements was attached. The experiments were carried out in the Faraday geometry ($B \| k \| [111]$) in magnetic fields up to 6 T at 4.2 K. Far infrared (FIR) radiation is incident on the sample and the reflected beam is detected by a liquid-He cooled Ge bolometer. For $Pb_{1-x}Eu_xTe$ epilayers on $BaF_2$ substrates, thermal-expansion mismatch strain (about $1\times10^{-3}$) pushes the oblique valleys ($o$ valleys) up a few meV with respect to the longitudinal valley ($l$ valley),[40] and thus more electrons populate the longitudinal valley than the oblique valleys. For sufficiently low-carrier concentrations, it is possible that all the carriers are located only in the longitudinal valley. (The absolute value of the strain in the epilayer depends also on the Eu content.) For samples with sufficiently low carrier concentrations, cyclotron resonance can only be observed for the carriers in the longitudinal valley of $Pb_{1-x}Eu_xTe$. For $Pb_{1-x}Eu_xTe$ samples used in this work, the carrier concentrations range from $2.2\times10^{16}$ to $5.0\times10^{16}$ cm$^{-3}$, except for sample No. 143 with a high carrier concentration of $4\times10^{17}$ cm$^{-3}$ (see Table I). For all $Pb_{1-x}Eu_xTe$ epilayers studied in this work, dips in the reflectivity spectra are observed due to magnetic-field-induced dielectric anomalies (DA's) involving electrons in the longitudinal valley. DA's arise in the range of frequencies close to the zeros of the total dielectric function.[40–42] They are located in a spectral regime, where normally (i.e., without magnetic field) the sample is totally reflecting.[40]

For the PbTe sample No. 127 ($x=0$) which has the lowest strain and for the $Pb_{1-x}Eu_xTe$-sample No. 143 which has the highest electron concentration, DA's involving electrons in the *oblique* valleys are also observed. Since the DA's cause the strongest spectral features accompanying the actual cyclotron resonance (CR) positions, in a magnetoreflectivity or magnetotransmission spectrum, an unambiguous determination of CR is only possible by a numerical fit to the observed spectra.[40,42]

## III. THEORETICAL BACKGROUND

The optical response of a sample is commonly described by a frequency-dependent dielectric function. In a magnetic field, in Faraday or Voigt configuration, the free-carrier dielectric function becomes a tensor.[41] This tensor has been derived for PbTe by several authors for the many-valley case[40–42] for light propagation along the [111] direction, including phenomena due to finite damping. In Faraday configuration and for $\mathbf{B} \| [111]$, the dielectric function including the polar-phonon contribution to the dielectric function (the TO mode is infrared active in the rocksalt crystal structure) is given by[42]

$$\begin{aligned}\varepsilon^{\pm} = \varepsilon_\infty + \frac{\varepsilon_\infty(\omega_{\mathrm{LO}}^2-\omega_{\mathrm{TO}}^2)}{\omega_{\mathrm{TO}}^2-\omega^2-i\gamma\omega} - \frac{n^{(l)}e^2}{\varepsilon_0 M_\perp^-} \\ \times \frac{\omega \mp \omega_c^{(l)} - i\omega_{\tau 1}}{\omega[(\omega \mp \omega_c^{(l)})^2+\omega_{\tau 1}^2]} - \frac{n^{(o)}e^2}{\varepsilon_0 m_0} \\ \times \frac{[a(\omega+i\omega_{\tau 2}) \pm b\omega_c^{(l)}][\omega^2-(\omega_c^{(o)})^2-\omega_{\tau 2}^2-2i\omega\omega_{\tau 2}]}{\omega\{[\omega^2-(\omega_c^{(o)})^2-\omega_{\tau 2}^2]^2+4\omega^2\omega_{\tau 2}^2\}},\end{aligned} \tag{1}$$

where

$$\omega_c^{(l)} = \frac{eB}{M_\perp^-} \quad \text{(CR frequency for longitudinal valley)}, \tag{2}$$

$$\omega_c^{(o)} = \frac{eB}{M_\perp'^-} \quad \text{(CR frequency for oblique valleys)}, \tag{3}$$

$$\frac{1}{M_\perp'^-} = \frac{1}{M_\perp^-}\left(\cos^2\theta + \sin^2\theta \frac{M_\perp^-}{M_\parallel^-}\right)^{1/2} = \frac{1}{3M_\perp^-}\left(1+8\frac{M_\perp^-}{M_\parallel^-}\right)^{1/2}, \tag{4}$$

$$a = \frac{m_0}{12}\left(\frac{4}{M_\parallel^-}+\frac{5}{M_\perp^-}\right), \tag{5}$$

$$b = \frac{m_0}{12}\left(\frac{8}{M_\parallel^-}+\frac{1}{M_\perp^-}\right), \tag{6}$$

$\omega_{\mathrm{TO}}$ is the transverse-optic-phonon frequency, and $\omega_{\tau 1}$ and $\omega_{\tau 2}$ denote the free-carrier damping frequencies in the [111] longitudinal valley and in the three obliquely oriented valleys, respectively. $n^{(l)}$ and $n^{(o)}$ are the carrier concentrations in the longitudinal and oblique valleys. The superscripts ''$-$'' and ''$+$'' label conduction bands and valence bands. The cyclotron masses $M_{\perp}^{-}$ and $M_{\parallel}^{-}$ denote the principal masses of the energy ellipsoids of the conduction and the valence band. $M_{\perp}'^{\,-}$ is related to the oblique valley ellipsoid and combines in dependence on the inclination angle $\theta$ both interband momentum matrix elements $2P_{\perp}^2/m_0$, and $2P_{//}^2/m_0$.[43] $\theta$ is the angle between the magnetic-field direction and the main axis of the valleys, i.e., $\cos\theta=1$ for the longitudinal valley and $\cos\theta=1/3$ for the three oblique valleys. For a nonvanishing magnetic field **B**, a detailed calculation of $M_{\perp}^{-}$ and $M_{\perp}'^{\,-}$ including the nonparabolicity of energy bands is given in Ref. 43.

The dielectric function as introduced above does not include the Fröhlich electron-LO-phonon interaction. The quantum-mechanical treatment of lowest order (= one phonon) electron-phonon interaction was specially applied for single-valley polar semiconductors like InSb.[44–46] Vogl and Kocevar[47] have calculated the correction for the real and imaginary part of the dielectric function of PbTe for finite population of the valleys and compared it with experimental results of Burkhard, Bauer, and Zawadzki.[42] In the following we adopt Harper's one-LO-phonon model for InSb (Ref. 44) and expand it to the many-valley semiconductor PbTe. The dielectric function for the Faraday geometry is of the form

$$\varepsilon^{\pm}=\varepsilon_{\infty}+\frac{\varepsilon_{\infty}(\omega_{\mathrm{LO}}^2-\omega_{\mathrm{TO}}^2)}{\omega_{\mathrm{TO}}^2-\omega^2-i\gamma\omega}\mp\frac{n^{(l)}e^2}{\varepsilon_0 M_{\perp}^{-}}\frac{1}{\omega Z^{\pm}(\omega)}\mp\frac{n^{(o)}e^2}{\varepsilon_0 M_{\perp}'^{\,-}}\frac{1}{\omega Z'^{\pm}(\omega)},\tag{7}$$

where the superscripts ''$\pm$'' attached to $\varepsilon^{\pm}$ and $Z^{\pm}$ refer to the response to right-hand $(+)$ and left-hand $(-)$ circularly polarized light, whereas the superscript ''$-$'' along with $M_{\perp}^{-}$ and $M_{\perp}'^{\,-}$ stands for the conduction band in the notation used for lead salts. $Z^{\pm}(\omega)$ and $Z'^{\pm}(\omega)$ are complex impedances, which explicitly contain the electron-LO-phonon interaction, and are distinct for the longitudinal and oblique valley, respectively. Taking $Z^{\pm}(\omega)=X(\omega)\pm iY(\omega)$, $X(\omega)$ is related to the frequency shift, $Y(\omega)$ to the line broadening of the cyclotron resonance line. Both $X$ and $Y$ are discontinuous as $\omega$ passes through $\omega_{\mathrm{LO}}$:

For $\omega<\omega_{\mathrm{LO}}$,

$$Y(\omega)=0,\tag{8}$$

$$X(\omega)=\omega-\omega_c-\alpha\omega_{\mathrm{LO}}\left(\frac{\omega_{\mathrm{LO}}}{\omega_c}\right)^{1/2}\mathrm{P}\int_0^{\infty}\left(\frac{1}{x}-\frac{1}{a}\right)\frac{x^3e^{-x^2}}{x^2-a^2}\,dx,\tag{9}$$

where $\omega_c$ denotes the corresponding cyclotron resonance frequency, $a^2=(\omega_{\mathrm{LO}}-\omega)/\omega_c$, and $x$ is the variable of integration. P takes the principal value of the integral. To include a finite damping even for $\omega<\omega_{\mathrm{LO}}$ a constant damping parameter $\gamma'$ is assumed for $\omega<\omega_{\mathrm{LO}}$ instead of $Y(\omega)=0$ according to Eq. (8).

For $\omega>\omega_{\mathrm{LO}}$,

$$X(\omega)=\omega-\omega_c-\alpha\omega_{\mathrm{LO}}\left(\frac{\omega_{\mathrm{LO}}}{\omega_c}\right)^{1/2}\mathrm{P}\int_0^{\infty}\frac{x^2e^{-x^2}}{x^2-(\omega-\omega_{\mathrm{LO}})/\omega_c}\,dx,\tag{10}$$

$$Y(\omega)=\frac{1}{2}\alpha\omega_{\mathrm{LO}}\left(\frac{\omega}{\omega_{\mathrm{LO}}}-1\right)^{-1/2}\mathrm{P}\int_0^{\infty}\frac{xe^{-x}}{x+(\omega-\omega_{\mathrm{LO}})/\omega_c}\,dx,\tag{11}$$

where $\alpha$ is the 3D Fröhlich coupling constant given by

$$\alpha=\frac{e^2}{4\sqrt{2}\pi\varepsilon_0}\left(\frac{1}{\varepsilon_{\infty}}-\frac{1}{\varepsilon_0}\right)\left(\frac{M_{\perp}^{-}}{\omega_{\mathrm{LO}}\hbar^3}\right)^{1/2}.\tag{12}$$

For the oblique valleys, the mass in Eq. (12) should be replaced by $M_{\perp}'^{\,-}$. For the longitudinal and oblique valleys of PbTe, the Fröhlich constant at $B=0$ is $\alpha=0.12$ and $\alpha'=0.18$, respectively. For $Pb_{1-x}Eu_xTe$, it increases with Eu content, due to the increase of the effective mass (see below) and the decrease of $\varepsilon_{\infty}$ with increasing Eu content.[35]

Finally we address the problem of the polaron correction in a material with a many-valley band structure. The anisotropic effective mass in PbTe-related compounds must be corrected for electron-LO-phonon interaction in the following way. The undressed masses differ by a factor of 10, i.e., the longitudinal mass is ten-times heavier than the transverse mass. Dressing by long-wave LO phonons of $q$ vectors near the center of the Brillouin zone yields a slight isotropization of the masses. We follow an analysis of Pekar and co-workers[18,19] and Larsen,[20] where the influence of electron-phonon interaction onto mass anisotropy is explicitly analyzed. The final result for the dressed masses in the 3D case is

$$\frac{1}{\mu_{\perp}}=\frac{1}{M_{\perp}}\left[1-\frac{\alpha}{6}\varphi_{\perp}\left(\frac{M_{\parallel}}{M_{\perp}}\right)\right],\tag{13}$$

$$\frac{1}{\mu_{\parallel}}=\frac{1}{M_{\parallel}}\left[1-\frac{\alpha}{6}\varphi_{\parallel}\left(\frac{M_{\parallel}}{M_{\perp}}\right)\right].\tag{14}$$

$M_i$ are the *undressed* 3D masses, $\mu_i$ the masses corrected for LO-phonon interaction. The anisotropy parameters $\varphi_i$ are derived in Refs. 18,19 for a mass anisotropy of $\approx 10$ being $\varphi_{\perp}=1.6886$ and $\varphi_{\parallel}=0.5988$. From Eqs. (13) and (14), we obtain instead of the undressed mass $M_{\perp}=0.22m_0$ the polaron mass $\mu_{\perp}=0.0228m_0$, and $\mu_{\parallel}=0.243m_0$ for $M_{\parallel}=0.22m_0$. Correspondingly the Fröhlich parameters according to Eq. (12) are changed from

$$\alpha_{\perp}=0.1264 \quad \text{to} \quad \alpha_{\perp}=0.1287,$$

$$\alpha_{\parallel}=0.1907 \quad \text{to} \quad \alpha_{\parallel}=0.1940.$$

It turns out that these corrections are rather small. We would like to point out that Larsen[48] has *explicitly* taken into account the electron-phonon coupling into the $\mathbf{k}\cdot\mathbf{p}$ matrix Hamiltonian for isotropic (but nonparabolic) bands. Since there is no weak-coupling theory for polarons in nonparabolic anisotropic bands, we have restricted ourselves to the use of Harper's perturbative approach, starting with un-

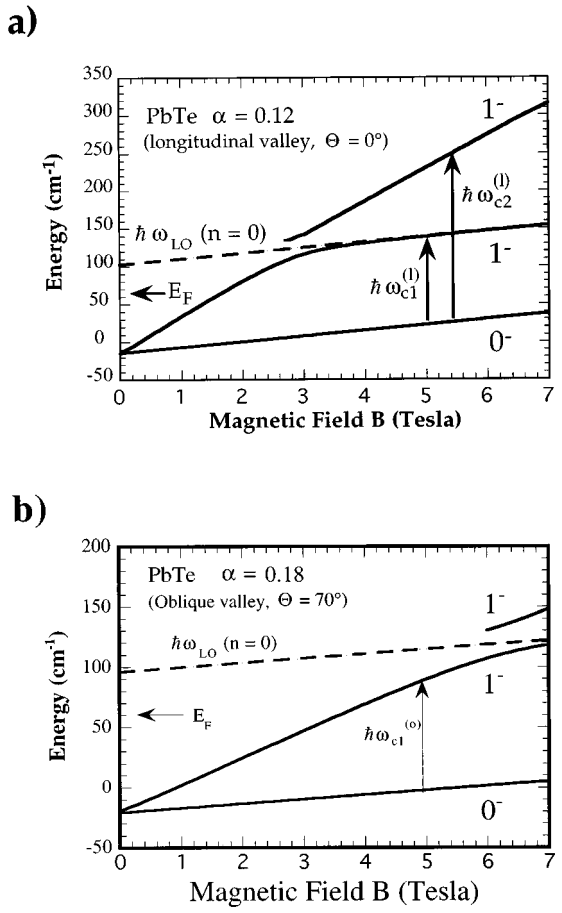


FIG. 1. Coupled electron-LO-phonon energy levels of PbTe as a function of magnetic field for the longitudinal (a) and oblique (b) valleys. Solid lines are for ''spin-down'' levels, while dashed lines are for ''spin-up'' levels. The Landau levels are corrected for polaron-mass enhancement (Ref. 16). The lowest Landau levels are obtained from Ref. 43. The dashed-dotted line shows the LO-phonon offset. Arrows indicate split cyclotron resonances.

dressed masses. Our treatment of the polaron corrections in the anisotropic parabolic bands of the IV-VI compounds is thus in the sense of Larsen's model not sufficient. As stated above, the corresponding changes in the Fröhlich parameters $\alpha$ are so small, that our treatment is at least plausible.

In this spirit, in the expressions for the dielectric function, for the cyclotron resonance energies $\hbar\omega_c$ in Eqs. (9)–(11), the corresponding nonparabolic energies calculated from the $\mathbf{k}\cdot\mathbf{p}$ model in a magnetic field were inserted, i.e., using essentially the undressed expressions for the masses for both the longitudinal and the oblique valleys. Thus, in all the fits of the experimental magnetoreflectivity spectra we used nonparabolic bare masses for both types of valleys and added the polaron correction as a perturbation to the bare band parameters in the spirit of Harper's model.

The energy of LO-phonon coupled Landau levels was obtained by neglecting the broadening $Y(\omega)$ and solving for the zeros of $X(\omega)$. The results are shown for PbTe in Figs. 1(a), (b). For the longitudinal valley [Fig. 1(a)] the $n=1^-$ spin level becomes double valued for $B>2.7$ T, as can be seen by the split solid line. If one neglects any population effect of the lowest (unsplit) Landau spin level $0^-$, the CR splits also into two resonances for a magnetic field $B>2.7$ T. We denote the branch with the lower CR energy by $\omega_{c1}^{(l)}$, and the other by $\omega_{c2}^{(l)}$. The dashed line is the LO-phonon offset energy added to the lowest Landau level, which should visualize the pinning of the lower CR branch to $(1/2)\hbar\omega_c+\hbar\omega_{\mathrm{LO}}$. The corresponding CR transitions for the upper spin state (superscript $+$) are not shown for simplicity. Note, that the extrapolated fan chart of Fig. 1(a) for $B\rightarrow 0$ does not emerge from zero energy, since for the 3D case the polaron-dressed mass correction $m^*\rightarrow m^*(1+\alpha/6)$ shifts the CR energy to a lower energy than is expected from an undressed CR.

For the oblique valleys [Fig. 1(b)] the crossover between the zero-phonon dispersion curve and the $(n=1^-)$-Landau level takes place at a higher magnetic field $B=6$ T, which reflects the mass increase $(M_{\perp}'^{-}>M_{\perp}^{-})$ of the oblique valley. The calculations take into account the distinct Fröhlich parameters $\alpha,\alpha'$ for both valley types, and include nonparabolicity effects.

For the remainder of this chapter we shall transfer the one-phonon model of electron-phonon coupling to the 2D case. The influence of (i) possible screening and (ii) of the Landau-level occupation effects on the resonant interaction with 2D polarons will be discussed later on. The dielectric function for a 2D electron gas in a magnetic field is given by[49–51]

$$\varepsilon(\omega)=\varepsilon_\infty+\frac{\varepsilon_\infty(\omega_{\mathrm{LO}}^2-\omega_{\mathrm{TO}}^2)}{\omega_{\mathrm{TO}}^2-\omega^2-i\gamma\omega}+\frac{i\sigma(\omega)}{\omega\varepsilon_0}, \tag{15}$$

where $\sigma$ is the dynamical conductivity of a 2D electron gas in a magnetic field.[17,26] For the PbTe case, the relevant equations were given by Pichler, Bauer, and Clemens,[49]

$$\sigma^{\pm}(\omega)=\frac{n_s e^2}{M_{\perp(2\mathrm{D})}^{-}}\,\frac{\omega_\tau+i(\omega\pm\omega_c)}{\omega_\tau^2+(\omega\pm\omega_c)^2}. \tag{16}$$

$\omega_c$ is the cyclotron frequency, $\omega_\tau$ the damping parameter. $n_s$ is the 2D electron gas density. The $\pm$ signs denote the right- or left-hand polarization state of radiation.

For an applied magnetic field parallel to the sample growth direction, i.e., for the Faraday configuration $B\|k\|$ [111], the eigenenergies have been calculated in the framework of the envelope function approximation (EFA) following the procedure outlined by Kriechbaum *et al.*[52] Whereas for the [111] (longitudinal) valley the analysis is straightforward, the calculation of the magnetoelectric levels for the oblique levels is much more elaborate. For all our MQW samples, the carrier concentration is such that only the lowest electric subband associated with the longitudinal valley is populated $(E_1^l)$, i.e., also the lowest oblique QW subband $(E_1^o)$ is not populated by electrons, where $l$ is the index of electric quantization (subbands in the QW's, $l=1,2,\ldots$), $n$ is the Landau index $(n=0,1,2,\ldots)$ of magnetic quantization. $E_l$ are evaluated using an envelope function calculation assuming a type-I conduction-band offset of $[E_g(\mathrm{Pb_{1-x}Eu_xTe})-E_g(\mathrm{PbTe})]/E_g(\mathrm{Pb_{1-x}Eu_xTe})=0.55$.[36,37]

For the calculation of the eigenenergies as a function of the magnetic field $E_n(B)$, the band parameters of bulk PbTe (Ref. 43) and of bulk $Pb_{1-x}Eu_xTe$ (Ref. 53) are used. From the effective band-gap enhancement due to the formation of the electric subbands, the 2D CR mass in the PbTe

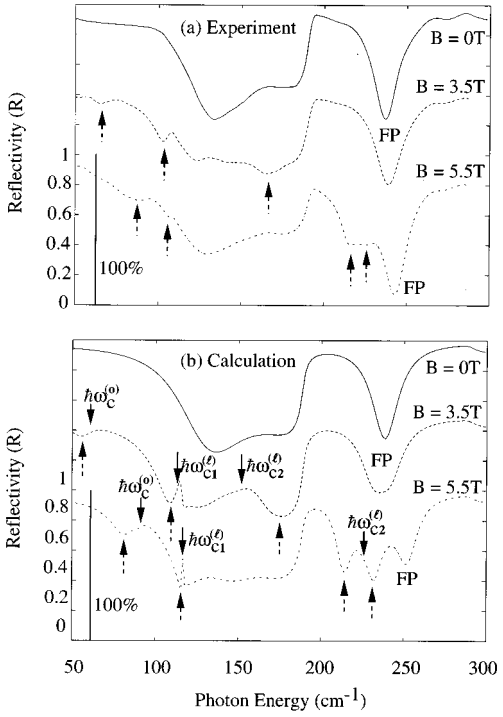


FIG. 2. Experimental (a) and calculated (b) reflectivity spectra of PbTe No. 127 at 4.2 K for $B=0$, 3.5, and 5.5 T. CR energies and dielectric anomalies are indicated by full and dashed arrows, respectively. FP denotes the Fabry-Perot fringes. For clear presentation, the spectra for $B=3.5$ and 0 T are shifted up by 0.5 and 1, respectively. No adjustable band parameters are used in the calculation.

QW's becomes larger than the corresponding PbTe 3D CR mass $M_{\perp}^{-}$. Since the EFA calculation is based on the $(4\times4)$ $\mathbf{k}\cdot\mathbf{p}$ matrix Hamiltonian for PbTe like compounds,[54] it includes all nonparabolicity corrections, of course also for finite magnetic fields. The magnetic-field dependence of the 2D cyclotron mass follows from the eigenenergies, and is obtained from

$$M_{\perp(2D)}^{-}(B)=\frac{\hbar eB}{E_2(B)-E_1(B)}, \tag{17}$$

where the indices denote adjacent Landau levels.

For the simulation of the magnetoreflectivity spectra at fixed magnetic field first information on the background dielectric function of the $Pb_{1-x}Eu_xTe$ barrier layers and of the $Pb_{1-x}Eu_xTe$ buffer layer is needed. This is derived from independent FTIR transmission measurements on $Pb_{1-x}Eu_xTe$ single epilayers using the method described in Ref. 36. For a given dielectric function and thickness of each individual layer (including the substrate, the buffer layer, the PbTe QW layers and the $Pb_{1-x}Eu_xTe$ barrier layers), the magnetoreflectivity spectra of the multilayer MQW samples can be calculated as a function of magnetic field using the transfer-matrix method[55] as outlined by Pichler, Bauer, and Clemens[49] and Kim *et al.*[51]

## IV. RESULTS AND DISCUSSIONS

### A. $Pb_{1-x}Eu_xTe$ ($0\leqslant x\leqslant 3.43\%$) single epilayers

In Fig. 2(a) experimental reflectivity spectra from a PbTe epilayer (sample No. 127) are shown for magnetic fields

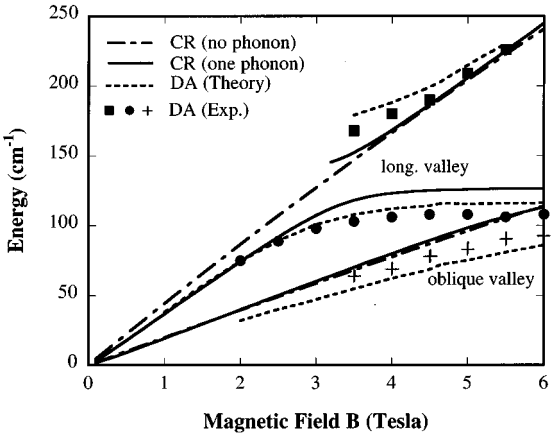


FIG. 3. Fan chart for PbTe No. 127 showing (1) cyclotron resonance energies with and without taking into account the electron-LO-phonon interaction and (2) the experimentally observed and calculated dielectric anomalies (DA's) associated with cyclotron resonances. Results are for the longitudinal ($l$) and oblique ($o$) valleys. All band parameters used in the calculation are taken from Ref. 29.

$B=0$, 3.5, and 5.5 T. For $B=0$ and 3.5 T, the traces are shifted upwards by 1 and 0.5, respectively. For $B=0$, the effective plasma frequency $\omega_p^*$ is close to the LO-phonon energy (117 cm$^{-1}$) of PbTe. The sharp increase of the reflectivity at about 190 cm$^{-1}$ indicates the TO-phonon frequency of the $BaF_2$ substrate.[42] The first Fabry-Perot (FP) fringe appears at 240 cm$^{-1}$, its position depends essentially on the thickness of the epilayer. In the presence of a magnetic field, dips in the reflectivity spectra appear due to dielectric anomalies from a zero of the dielectric function, which are indicated by dashed arrows. Taking the dielectric function of Eqs. (7)–(11) and applying the transfer-matrix method[55] for the propagation of electromagnetic fields through the epilayer and substrate, the reflectivity spectra are calculated for $B=0$, 3.5, and 5.5 T. Since for the experiments nonpolarized FIR light was used, the reflectivity is calculated as an average of reflectivities for left- and right-hand circularly polarized light. In the calculation, the band parameters of PbTe are taken from the literature.[40] For $BaF_2$ the following phonon parameters are used: $\omega_{TO}=189$ cm$^{-1}$, $\omega_{LO}=290$ cm$^{-1}$, $\varepsilon_0=1.93$, and $\gamma=3$ cm$^{-1}$. The calculated results of reflectivity spectra are shown in Fig. 2(b) in which the CR positions are indicated by full arrows, and the dielectric anomalies by dashed arrows. A splitting of the longitudinal ($\swarrow$) valley CR ($\hbar\omega_{c1},\hbar\omega_{c2}$) due to Fröhlich electron-phonon interaction is indeed required to reveal the experimentally observed features. The CR for the oblique ($o$) valley appears at lower frequency due to an increased effective mass. From the fits to the reflectivity spectra the effective masses are extracted, taking into account the nonparabolicity of the band structure.[43] They depend on the magnetic field due to the polaron effect and they determine the CR frequency $\omega_c$ and the Fröhlich constant $\alpha$ according to Eqs. (2) and (3) and Eq. (12).

In Fig. 3, the experimentally observed and calculated cyclotron resonance energies and the energy positions of dielectric anomalies are plotted as a function of magnetic field for the PbTe sample No. 127 (which has a mobility

TABLE III. Parameters used for the calculation of the magnetoreflectivity spectra for $Pb_{1-x}Eu_xTe$.

| Sample No. | $n(l)/n$ [a] | $\omega_{LO}$ | $\omega_{TO}$ | $\alpha$ [b] | $\gamma$ | $\gamma'$ | $\varepsilon_0$ [c] | $\varepsilon_\infty$ [d] |
|---|---|---|---|---|---|---|---|---|
| | (%) | ($cm^{-1}$) | ($cm^{-1}$) | | ($cm^{-1}$) | ($cm^{-1}$) | | |
| No. 127 | 25 | 117 | 18 | 0.120 | 15 | 5 | 1521 | 36 |
| No. 143 | 68 | 117 | 18 | 0.147 | 18 | 5 | 1407 | 33.3 |
| No. 199 | 100 | 117 | 18 | 0.151 | 20 | 5 | 1399 | 33.1 |
| No. 114 | 100 | 118 | 18 | 0.167 | 20 | 5 | 1354 | 31.5 |
| No. 145 | 100 | 120 | 18 | 0.198 | 25 | 5 | 1258 | 28.3 |

[a] $n^{(l)}/n$ is the percentage of carriers in the longitudinal valley.
[b] For longitudinal valley only and for low magnetic field.
[c] Obtained from the $L$-$S$-$T$ relation: $\varepsilon_0=\varepsilon_\infty\ (\omega_{LO}/\omega_{TO})^2$.
[d] Extrapolated from Ref. 19.

$\mu=4.65\times10^5$ $cm^2/V\,s$ at $T=20$ K). We observed also the upper branch $\hbar\omega_{c2}$ of CR for electrons in the longitudinal valley. The lower branch $\hbar\omega_{c1}$ of the CR pins to the LO-phonon frequency (at about 117 $cm^{-1}$, this value increases slightly with increasing Eu concentration) at high magnetic fields. Such a pinning effect is also expected for the lower branch of CR in oblique valleys but their CR transition is only close to the LO-phonon frequency at magnetic fields $B$ close to 6 T, and thus in the field range investigated, this upper branch is not visible.

As demonstrated in Ref. 7, the carrier mobility of $Pb_{1-x}Eu_xTe$ samples drops dramatically with increasing Eu content, i.e., for $x=2.5\%$ the electron mobility at liquid helium temperatures is already as low as $2\times10^4$ $cm^2/V\,s$ (see Table I). It turns out that for the $Pb_{1-x}Eu_xTe$ epilayers, only the lower branch of the CR line is observable, probably due to the much stronger damping than in pure PbTe. It is evident that the positions of the DA dips of course do not coincide with corresponding CR energies. The phonon and Fröhlich parameters and the percentual population of the longitudinal valley, which are used in the calculations, are listed in Table III. The carrier transport and band parameters, the momentum matrix elements and effective masses in the framework of a two-band model of IV-VI-compound semiconductors are listed in Table IV for all $Pb_xEu_{1-x}Te$ samples.

In Fig. 4(a), measured reflectivity spectra are shown for a $Pb_{1-x}Eu_xTe$ sample (No. 199, $x=0.0173$) for $B=0$ and 4 T. As mentioned previously, the electrons populate only the longitudinal valley for an electron concentration of $2.5\times10^{16}$ $cm^{-3}$, since the epilayer strain lifts the valley degeneracy at the $L$ points of the Brillouin zone. Consequently, only DA's for longitudinal valleys are observed. For $B=4$ T two DA dips associated with cyclotron resonance absorption are resolved. The calculated spectra using the model dielectric function Eq. (7) are shown in Fig. 4(b). From the numerical simulations it is found that one of the two DA dips, the one at higher photon energy disappears if the carrier concentration falls below $10^{16}$ $cm^{-3}$.

Similar results are obtained for the other $Pb_{1-x}Eu_xTe$ samples. A comparison between experimental and calculated fan charts is shown in Fig. 5 for samples No. 199 ($x=0.0173$) and No. 114 ($x=0.0245$). The CR frequencies with (full line) and without (dashed-dotted line) electron-LO-phonon interaction are plotted as a function of magnetic field. Note the excellent correspondence of calculated and measured DA positions.

For the $Pb_{1-x}Eu_xTe$ sample No. 143 ($x=0.013$) with a relatively high electron concentration of $4\times10^{17}$ $cm^{-3}$, also the oblique valleys are partly populated by electrons. Therefore, CR of electrons in the oblique valley is observed in the experiments. The momentum matrix elements as given in Table IV are somewhat different from the ones reported previously by Karczewski *et al.*,[56] but are similar to those of Geist *et al.*[53] Thus the energy ellipsoid in $k$ space for the lowest conduction band in $Pb_{1-x}Eu_xTe$ becomes somewhat more isotropic with Eu alloying than that of PbTe, an observation which is in agreement with recent interband magnetooptical experiments.[53]

In Tables III and IV the lattice and band parameters used for the calculation are listed for all $Pb_{1-x}Eu_xTe$ samples. The transverse effective masses as obtained from our CR measurements on the [111] valleys of $Pb_{1-x}Eu_xTe$ are a

TABLE IV. Two-band parameters of $Pb_{1-x}Eu_xTe$.

| Sample No. | $x$ (%) | $E_g$ (meV) | $\mu$ ($10^3$ $cm^2/V\,s$) | $2P_{\|\|}^2/m_o$ (eV) | $2P_\perp^2/m_o$ (eV) | $M_\perp^-$ ($m_o$) | $M_{\|\|}^-$ ($m_o$) |
|---|---|---|---|---|---|---|---|
| No. 127 | 0 | 189.7 | 465 (20 K) | 0.51 | 6.02 | 0.021 | 0.21 |
| No. 143 | 1.30 | 248 | 50 | 0.5 | 5.3 | 0.026 | 0.25s |
| No. 199 | 1.73 | 267 | 100 | | 5.2 | 0.028 | |
| No. 114 | 2.45 | 299 | 3.1 (77 K) | | 4.8 | 0.031 | |
| No. 145 | 3.43 | 343 | 20 | | 4.0 | 0.035 | |
| Ref. 55 | 2.0 | 279 [a] | 30 (4 K) | 0.55 | 8.23 | 0.020 | 0.218 |

[a] According to the note added in proof, the calculated energy gap for $x=0.02$ is $E_g=279$ meV.

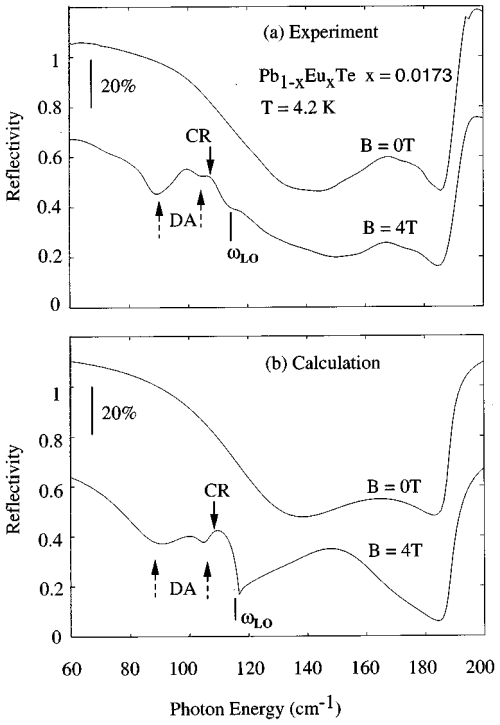


FIG. 4. Measured (a) and calculated (b) reflectivity spectra for $Pb_{1-x}Eu_xTe$ No. 199 for $B=0$ and 4 Tesla. CR's and associated dielectric anomalies DA's are indicated by full and dashed arrows, respectively.

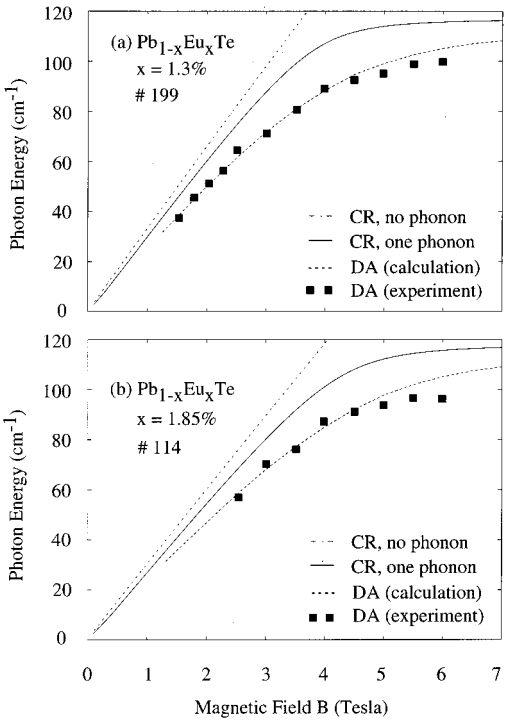


FIG. 5. Cyclotron resonance (CR) energies with and without electron-LO-phonon interaction versus magnetic field for the $Pb_{1-x}Eu_xTe$ single layers Nos. 199 and Nos. 114. In the experiments, CR manifests itself through dielectric anomaly (DA). Both calculated and measured DA are shown in the graph.

function of the Eu content $x$ and are plotted in Fig. 6. The transverse mass increases continuously with increasing $x$ from $0.021m_0$ for PbTe ($x=0$) to $0.035m_0$ for $x=0.0343$. The accuracy of the determination of the longitudinal mass from experiments with $B\|[111]$, i.e., from the cyclotron resonance of the carriers in the oblique valleys, is not very high and further experiments, in particular, with $B\|[110]$ would be needed. For Eu contents higher than $x=1.3\%$, the longitudinal mass could not be determined from the CR resonances at all, since the oblique valleys are not populated for the comparatively low-carrier concentrations (see Table I).

The analysis of the CR data shows that the transverse momentum matrix element $2P_\perp^2/m_0$ decreases with Eu content from 6.02 eV for PbTe to about 4.0 eV for $x=0.0343$ (in reasonable agreement with the analysis of magnetooptical interband investigations[53]), while the longitudinal momentum matrix element $2P_\|^2/m_0$ does not change significantly with Eu content at least up to $x=0.013$. For a $p$-type $Pb_{1-x}Eu_xTe$ sample ($x=0.02$, with a hole concentration of $7.5\times10^{17}$ cm$^{-3}$), Karczewski *et al.*[56] determined the effective hole masses from magnetotransmission experiments and derived values for the momentum matrix elements $2P_\perp^2/m_0$ and $2P_\|^2/m_0$. Their results are compared with ours in Table IV (last line) and in Fig. 8. For the transverse momentum matrix element Karczewski *et al.* quoted $2P_\perp^2/m_0=8.23$ eV, for $2P_\|^2/m_0=0.55$ eV (for $x=0.02$). Thus their results imply an increase of the mass anisotropy ratio $K$ for holes, whereas our results imply a slight decrease of $K$ for electrons. The discrepancy between their results for $2P_\perp^2/m_0$ and ours (8.23 vs 4.8 eV) as well as those by Geist *et al.*[53] is obvious. We find that the conduction-band transverse mass $M_\perp^-$ increases with Eu content, in agreement with the results of both Refs. 53 and 57. The origin for this discrepancy on $2P_\perp^2/m_0$ and $2P_\|^2/m_0$ can be manifold, and, in particular, we would like to stress that for the determination of the dependence of the effective masses on the composition $x$ for $Pb_{1-x}Eu_xTe$ from the cyclotron resonance experiments on just one type of carriers the variation of the energy gap of $Pb_{1-x}Eu_xTe$ with composition $x$ has to be known precisely in the investigated samples. Furthermore, information on the far band contributions to the effective masses are required as well (since these are essential, contributing of the order of 30%). We used measured values for $E_g$ from absorption data

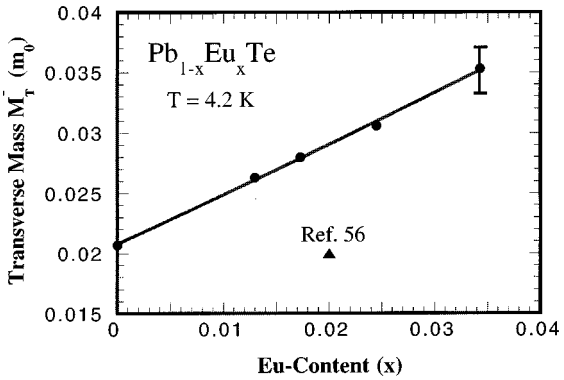


FIG. 6. The transverse effective masses for $Pb_{1-x}Eu_xTe$ as a function of Eu concentration $x$. Results of this work and those by Karczewski *et al.* (Ref. 56) are compared.

for the analysis of the CR data. The results for the $Pb_{1-x}Eu_xTe$ band parameters derived from a set of five samples using interband magnetooptical and CARS experiments with $x$ ranging from 0 up to 0.017 performed by Geist *et al.*[53] essentially confirm our own set of data derived from the CR, i.e., a steady decrease of $2P_{\perp}^2/m_0$ from its value for PbTe with increasing Eu content. Finally, we would like to mention, that $Pb_{1-x}Eu_xTe$ is a diluted magnetic semiconductor and thus electron-Eu exchange interaction[43,53,58] might influence the Landau-level energies as a function of the magnetic field. Recent coherent anti-Stokes Raman-scattering experiments, where the $g$ factors are measured directly have shown, that for electrons the exchange induced corrections are negligibly small, i.e., the exchange parameters $B$ and $b_1$ are just $5\pm3$ and $0.3\pm3$ meV, respectively. Thus, in particular, for the calculation of the electron CR transition energies, exchange-induced corrections can be neglected.

### B. PbTe/$Pb_{1-x}Eu_xTe$ quantum well samples

The motivation to perform cyclotron resonance experiments on PbTe/$Pb_{1-x}Eu_xTe$ quantum-well samples was twofold:

(a) Due to the band nonparabolicity of the narrow gap PbTe a strong dependence of the 2D cyclotron masses on the PbTe well width can be expected, and

(b) since the 2D CR transition energies can be tuned through the LO-phonon energy in the range of magnetic fields accessible, it is obvious that one can study the resonant 2D-electron LO-phonon interaction in PbTe/$Pb_{1-x}Eu_xTe$ QW's.

To address the first problem, magnetoreflectivity spectra of several PbTe/$Pb_{1-x}Eu_xTe$ MQW samples were measured in the Faraday geometry. The four samples studied are listed in Table II, and had quite similar Eu contents (3.2–3.9%) in the $Pb_{1-x}Eu_xTe$ layers and thus not very different barrier heights. The $Pb_{1-x}Eu_xTe$ barrier width was chosen to be sufficiently long (486–648 Å), in order to ensure negligible overlap of the wave functions for carriers confined in the $n=1$ or 2 electric subbands of the PbTe wells. The PbTe well width ranged from 62 to 118 Å, leading to a change of the lowest interband transition energy $(1\text{-}1)^{\ell}$ between confined electron and hole levels from 203 to 224 meV.

For solving the second problem, magnetoreflectivity measurements were performed on the PbTe/$Pb_{1-x}Eu_xTe$ MQW samples in the field range between 2 and 6 T. As described in Sec. II, the MQW structures were deposited on $Pb_{1-x}Eu_xTe$ buffers. The use of the comparatively thick $Pb_{1-x}Eu_xTe$ buffer (about 5 $\mu$m thick, see Table II), which has the identical Eu content as the barrier layers, induces in the buffer layer, however, a parallel channel of 3D electrons.

All MQW samples investigated were characterized by interband absorption measurements and by the midinfrared photoconductivity spectra in the absence of a magnetic field. The photoconductivity spectra show clearly the (1-1) interband transitions within the QW structures involving electrons both in the longitudinal valley ($l$) and oblique valleys ($o$).[36] The $(1\text{-}1)^o$ interband transition energy is considerably higher than the $(1\text{-}1)^l$ interband transition energy, in good agreement with envelope function approximation (EFA) calculations.[36] The onset of the photoconductivity spectrum

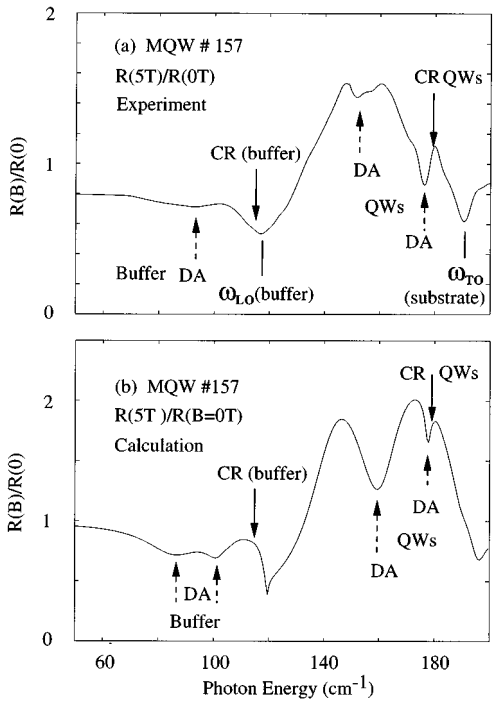


FIG. 7. Comparison between experimental (a) and calculated (b) $R(B=5\ \text{T})/R(B=0\ \text{T})$ spectra for PbTe/$Pb_{1-x}Eu_xTe$ MQW No. 157.

(taken at $T=4.2$ K) indicates that the lowest $1^o$ electric subband corresponding to the oblique valleys of the conduction band is not populated by electrons, otherwise the $(1\text{-}1)^l$ interband transition would not be observed in the photoconductivity experiments. Therefore, only the first subband of the longitudinal valley in the conduction band of the PbTe QW's is populated by carriers in all four samples listed in Table II. In the $Pb_{1-x}Eu_xTe$ buffer layers with a typical width of about 5 $\mu$m, a parallel electron channel is present, which can unfortunately not be avoided. Also there, only the longitudinal valley is populated with electrons.

As a consequence the magnetoreflectivity spectra as a function of the wave number with the applied magnetic field as a parameter show features associated with the 2D cyclotron resonance of electrons in the lowest electric subband of the longitudinal valley as well as a 3D cyclotron resonance of electrons in the longitudinal [111] valley in the $Pb_{1-x}Eu_xTe$ buffer layer, which have a much higher transverse effective mass. Due to the background dielectric function associated with the presence of the substrate, of the buffer and the barrier layers, the cyclotron resonance appears shifted with respect to reflectivity dips, which are in the following denoted by ''dielectric anomalies'' (DA's) despite the fact that not all dips are associated with zeros of the total dielectric function.

In order to enhance the magnetic-field-induced signatures in the reflectivity spectra, normalized data $R(B)/R(B=0)$ are shown in Fig. 7(a) for the MQW sample No. 157. In Fig. 7(b) calculated normalized reflectivity data for this sample are shown for comparison and for identification. The dips from the DA's and the cyclotron resonance positions can be assigned by inspection of the simulation Fig. 7. As expected there is just one cyclotron resonance due to the 2D electrons

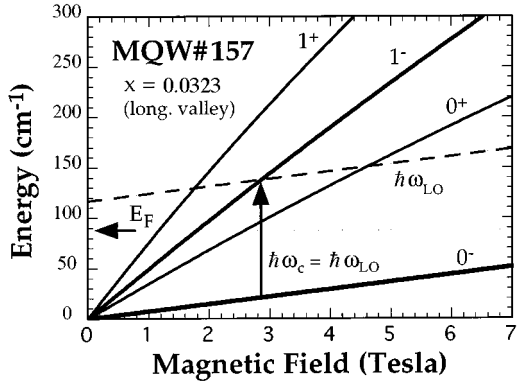


FIG. 8. The Landau levels attached to the lowest electric subband ($E_1$) of the longitudinal [111] valley in the PbTe QW's for PbTe/$Pb_{1-x}Eu_xTe$ MQW sample No. 157. The Landau levels are corrected for polaron-mass enhancement (Ref. 16). The zero energy is at the bottom of the QW's.

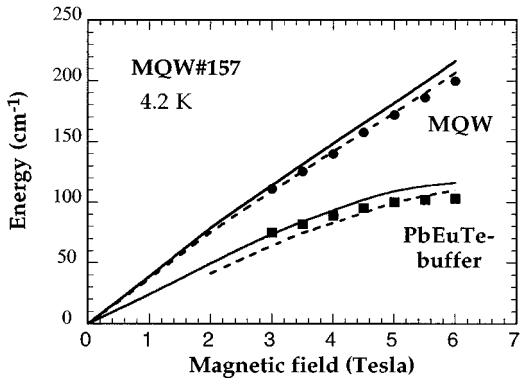


FIG. 9. Magneto-optical transition energies for PbTe/$Pb_{1-x}Eu_xTe$ MQW No. 157, showing the experimental and calculated dielectric anomalies (DA's) and cyclotron resonance (CR) energies as a function of magnetic field for both the electrons in the PbTe QW's and in the $Pb_{1-x}Eu_xTe$ buffer layer structures.

in the PbTe QW layers. However, it is preceded by more than one dip at lower wave numbers in the $R(B)/R(0)$ spectrum [designated by ''DA's'' in Figs. 7(a),(b)], which are simply caused by interference phenomena induced by the cyclotron resonance.

In the simulation in Fig. 7(b) we have used the magnetic-field dependence of the dielectric functions for the $Pb_{1-x}Eu_xTe$ buffer layer and for the MQW stack on top of it. For the 2D carriers in the PbTe wells a 2D CR damping parameter $\omega_\tau$ of 1 $cm^{-1}$, was used, whereas the corresponding 3D CR damping parameter $\gamma$ for the electrons in the $Pb_{1-x}Eu_xTe$ buffer layer turns out to be 5 $cm^{-1}$ (below LO-phonon frequency). Thus the 3D CR damping parameter is five-times larger than that for the 2D carriers, which is in qualitative agreement with the differences in the Hall mobilities. In the photon energy region close to the LO-phonon frequency of PbTe (117 $cm^{-1}$), the lower branch of the DA's in the QW's is not well resolved, neither in the experiment nor in the calculation. In Fig. 8 we show the calculated Landau-level fan chart for sample MQW No. 157. For the $0^-$-$1^-$ CR transitions the crossover with $\hbar\omega_{LO}$ occurs at about 2.8 T.

The transition energies for the MQW sample No. 157 are plotted in Fig. 9. It is found that the DA dips at the higher frequencies are associated with the CR in the PbTe-QW's (full circles), being that they are very close to the CR energy. These transitions do not pin to the LO-phonon energy. The second one (full squares) follows in its behavior a polaron-cyclotron resonance with a tendency of pinning to the LO-phonon energy.

In Fig. 10 for four MQW samples as listed in Table II, the cyclotron resonance energies of the 2D carriers in the PbTe wells are shown as a function of the magnetic field $B$, as obtained from the fits to the magnetoreflectivity data. For carriers in the electric subband associated with the longitudinal [111] valley the electric and magnetic quantization are decoupled for $B\|$ [111]. Thus the cyclotron masses should follow a simple trend: the QW's with the smallest energy $E_{11}$ for the $(1\text{-}1)'$ transitions should have the highest cyclotron resonance energies because the transverse mass of the electrons in this level should be the smallest. The experimental data shown for the four MQW samples exhibit indeed this trend with the gap $E_{11}$: sample No. 157 has the highest CR energy and sample No. 151 the lowest one, while sample Nos. 148 and 156, which have an identical gap $E_{11}$ have nearly the same CR energies in between those of MQW Nos. 157 and 151. Furthermore, in particular, from the data of MQW No. 151 it is apparent that the 2D cyclotron resonance energies do not exhibit any significant pinning to the LO-phonon energy. For this sample, at 3.5 T the CR energy crosses the LO-phonon energy (117 $cm^{-1}$). Apparently the smooth dependence of the CR energies on magnetic field clearly shows that pinning is indeed negligible.

In Fig. 11 the increase of the transverse CR mass due to band nonparabolicity is shown, as deduced from the experimental CR data. Since the QW interband gap $E_{11}$ is the same and all other PbTe and $Pb_{1-x}Eu_xTe$ band parameters are nearly identical for MQW sample Nos. 148 and 156 (see Table II), the corresponding CR masses are also nearly equal. However, we want to point out that due to the far band contributions in the $(4\times4)$ $\mathbf{k}\cdot\mathbf{p}$ Mitchell and Wallis Hamiltonian as used for the EFA calculations[52] the cyclotron masses are of course determined not alone by $E_{11}$.

The CR of 3D electrons in the $Pb_{1-x}Eu_xTe$ buffer layer is affected by the Fröhlich electron-LO-phonon interaction

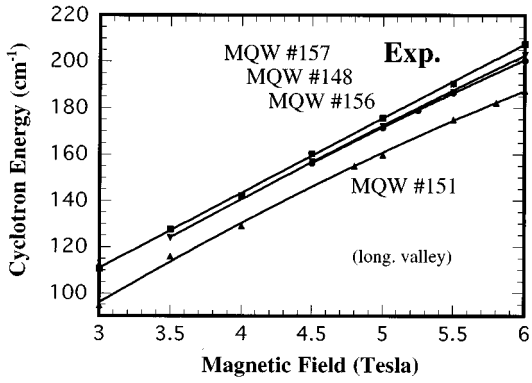


FIG. 10. Experimental values for the 2D CR transition energies as a function of magnetic field for four PbTe/$Pb_{1-x}Eu_xTe$ MQW structures (Nos. 157, 148, 156, 151). No resonant electron-LO-phonon interaction is observed.

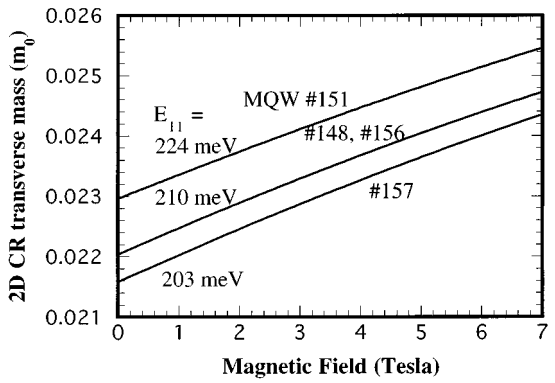


FIG. 11. 2D cyclotron masses of the four MQW's as derived from Fig. 10, as a function of the magnetic field.

(see, e.g., Fig. 9). Thus the lower branch of dielectric anomalies in Fig. 9 is interpreted as CR from the $Pb_{1-x}Eu_xTe$ buffer layer. The Eu content of the buffer layer $Pb_{1-x}Eu_xTe$ for sample Nos. 148, 151, 156, and 157 is $x =$ 0.0385, 0.035, 0.0336, 0.0323, respectively. Because the energy gap and in turn the 3D CR mass of bulk $Pb_{1-x}Eu_xTe$ increase with the Eu content, we expect that the CR energy of the buffer layers decreases correspondingly, which means that the position of the buffer-related DA's (squares) increases in energy for the sequence of sample Nos. 148, 151, 156, and 157. This fact is indeed observed.

## V. DISCUSSION

By the simple one-phonon-one-electron picture for the description of electron-LO-phonon interaction in a magnetic field, we neglected so far many-particle and population effects. It is known[43] that mass renormalization due to static or dynamic screening shifts the 2D polaron energy by a considerable amount. PbTe is quite a polar semiconductor and the screening radius in the Thomas-Fermi approximation has a value of 170 Å for $n^{2D}=10^{11}$ cm$^{-2}$ at 4.2 K, due to the rather tremendous static dielectric constant $\varepsilon_0 \approx 1400$. In this static limit, the screening radius becomes thus even larger than the typical quantum-well thickness of our QW samples. Therefore static screening is not probable in our short period QW samples ($d_w=62$–$118$ Å). If dynamic screening were significant, an increase of the polaron-shifted CR energies should be observed in the experiment. However, any observable shift in the PbTe QW cyclotron resonance energies does not occur (see Figs. 9,10) and thus its absence rules out dynamic screening.

Finally, we are left with the population effect of nonzero electron density. As worked out by Larsen[16] for electrons confined to a heterojunction, the polaron correction is subjected to a discontinuity as a function of the filling factor $\nu$ of the lower ($n=0$) Landau level at $\nu=1$ in a 2D electron system. The filling factor is defined as usual by

$$\nu = 2\pi n^{2D}\frac{\hbar}{M_{\perp}^{-}\omega_c} = \frac{n^{2D}h}{eB}. \tag{18}$$

We take for the 2D effective mass the value for the transverse mass in the longitudinal valley. The consequence of density-dependent polaron corrections is that in a given magnetic field, spin-up and spin-down cyclotron frequencies become slightly different when these spin states are unequally populated. In the case of PbTe we restrict the discussion to the spin level ($-$) of Fig. 1(a). For the expected polaron-split CR the field is $B=2.75$ T, which yields for a electron concentration of $10^{11}$ cm$^{-2}$ a filling-factor $1<\nu<2$. Thus this ($n=0$) Landau spin level is fully occupied, and virtual phonon transitions from the ($n=1$) Landau level to this level are forbidden by Pauli's exclusion principle. The same arguments hold also for the other ($+$) spin Landau levels of Fig. 1(a) for the whole range of magnetic fields in our experiments. Thus, for the rather highly populated quantum wells of PbTe in our MQW samples indeed we can rule out any observability of polaron corrections to the cyclotron resonance. To lower the filling factor to $\nu \leqslant 1$ at a magnetic field of $B=2.75$ T, the electron concentration should be decreased to about $n^{2D} \leqslant 6.5\times 10^{10}$ cm$^{-2}$ in the PbTe quantum wells. From such low-carrier MQW samples, not available at the time, polaron-corrected cyclotron resonance should be also observed in PbTe-based heterostructures. As shown in Fig. 11, obviously the observed increase of the transverse mass of the 2D electrons confined in the PbTe wells can be explained entirely and quantitatively by the band nonparabolicity on the basis of the ($4\times 4$) $\mathbf{k}\cdot\mathbf{p}$ Mitchell and Wallis Hamiltonian used for the EFA calculations.

## VI. SUMMARY

Systematic magnetoreflectivity experiments were performed on a series of $Pb_{1-x}Eu_xTe$ single epitaxial layers ($0 \leqslant x \leqslant 3.43$ %) in the far-infrared spectral region in a range where resonant electron-LO-phonon interaction occurs. These samples exhibit a bulklike behavior and show pinning phenomena. The cyclotron resonance (CR) transitions energies of electrons in the longitudinal and the oblique valleys (magnetic-field orientation $B\|[111]$) are pinned to the LO-phonon energy and become even split into two branches. In spite of the damping, even the upper branch of CR became observable in a PbTe epitaxial sample of sufficiently high electron mobility ($\mu \approx 5\times 10^5$ cm$^{-2}$/V s). In the frequency range of interest and in the range of magnetic fields applied, the cyclotron resonance frequency is smaller than the coupled LO-phonon-plasmon frequency of the IV-VI compound epilayer, or in the range of the reststraehlen region of the substrate. Thus, the cyclotron resonance is accompanied by dielectric anomalies and the experimental reflectivity dips do not coincide with the resonance positions. Therefore the experimental magnetoreflectivity data were analyzed with a model for the frequency and magnetic-field dependence of the dielectric function, were the electron-LO-phonon (Fröhlich) interaction was explicitly taken into account, based on Harper's model. This model starts with ''undressed'' masses, i.e., the Landau-level calculation is based on a rigid-lattice nonparabolic $\mathbf{k}\cdot\mathbf{p}$ model and includes the Fröhlich interaction in a perturbation approach. The polaron terms for both types of valleys consist of a Drude-like expression with the square plasma frequency as a prefactor and a complex impedance factor $1/\omega Z$. All phonon-assisted effects are included in $Z$ via the Fröhlich parameter $\alpha$, whereas the cyclotron frequencies are calculated as ''bare-''mass-derived quantities. The mass which appears in

the plasma frequency prefactor is also a bare mass derived from the rigid-lattice $\mathbf{k}\cdot\mathbf{p}$ model.

For the electrons in the two different types of valleys and thus with different cyclotron masses, pinning phenomena were clearly observed and quantitatively described. From our experiments and calculations on the cyclotron resonance transitions the two interband momentum matrix elements were obtained. Their numerical values compare favorably with a recent experimental determination of band parameters in $Pb_{1-x}Eu_xTe$ as a function of $x$, as derived from interband magneto-optical transitions and coherent anti-Stokes Raman-scattering experiments.

We have also investigated the cyclotron resonance of 2D electrons confined in the PbTe wells, with widths ranging from 62 to 118 Å, in PbTe/$Pb_{1-x}Eu_xTe$ MQW structures. In these samples just the lowest electric subband (associated with the longitudinal valley) was occupied and the relevant cyclotron mass for $B||[111]$ is the transverse mass. Due to the narrow gap of PbTe, nonparabolicity effects are clearly observed and quantitatively explained, based on the EFA model calculations. The 2D cyclotron resonance masses follow a trend according to which they are inversely proportional to the quantum-well gap, i.e., to the lowest interband transition energy $E_{11}$ between valence and conduction-electron subbands.

We did not find evidence for resonant 2D carrier-LO-phonon interaction for the electrons confined in the PbTe QW's in a series of PbTe/$Pb_{1-x}Eu_xTe$ samples investigated. This finding is attributed to finite-electron concentration effects and, in particular, to a filling of the lowest 2D Landau spin level $0^-$. Also arguments of static and dynamic screening were considered, but were ruled out for the explanation of the absence of polaron corrections to the 2D cyclotron resonance in PbTe quantum wells.

*Note added in proof.* Recently, the dependence of the $PB_{1-X}Eu_XTe$ energy gap on the Eu content $x$ has been checked and it was found that the previously established dependence (Refs. 1 and 35) has to be modified according to

$$E_g\ (\mathrm{meV}) = 189.7 + 0.48\left(\frac{T^2}{T+29}\right)[\mathrm{K}](1-7.56x) + 4480x.$$

## ACKNOWLEDGMENTS

We thank M. Kriechbaum for the EFA calculation of electronic subbands of the MQW samples, W. Zawadzki and F. Peeters for helpful discussions, and Y. S. Luo for assistance. This work was supported by Fonds zur Förderung der wissenschaftlichen Forschung under Grant No. 11557 by GME, and by the BMfWFK, Vienna, Austria.

*Present address: Department of Electronic Materials Engineering, Research School of Physical Sciences and Engineering, Australian National University, Canberra, ACT 0200, Australia.

[1] D. L. Partin, IEEE J. Quantum Electron. **QE-24**, 1716 (1988), and references therein.

[2] A. Ishida, H. Takashiba, T. Izutu, H. Fujiyasu, and H. Böttner, J. Appl. Phys. **75**, 619 (1994).

[3] G. Bauer, M. Kriechbaum, Z. Shi, and M. Tacke, J. Nonlin. Opt. Phys. Mater. **4**, 283 (1995).

[4] M. Tacke, Infrared Phys. Technol. **36**, 447 (1995).

[5] H. Zogg, A. Fach, C. Maissen, J. Masek, and S. Blunier, Opt. Eng. **33**, 1440 (1994).

[6] G. Springholz and G. Bauer, Phys. Rev. B **48**, 10 998 (1993), and references therein.

[7] G. Springholz, G. Ihninger, G. Bauer, M. M. Olver, J. Z. Pastaian, S. Romaine, and B. B. Goldberg, Appl. Phys. Lett. **63**, 1908 (1993).

[8] M. M. Olver, J. Z. Pastalan, S. E. Romaine, B. B. Goldberg, G. Springholz, G. Ihninger, and G. Bauer, Solid State Commun. **89**, 693 (1994).

[9] P. McCann, L. Li, J. Furneaux, and R. Wright, Appl. Phys. Lett. **65**, 2185 (1994).

[10] For a review see, e.g., R, Evrad, in *Polarons in Ionic Crystals and Polar Semiconductors*, edited by J. T. Devreese (North Holland, Amsterdam, 1972), p. 30.

[11] C. J. Summers, R. B. Dennis, B. S. Wherrett, P. G. Harper, and S. D. Smith, Phys. Rev. **170**, 755 (1968).

[12] L. Swierkowski, W. Zawadzki, Y. Guldner, and C. Rigaux, Solid State Commun. **27**, 1245 (1978).

[13] For a review see, e.g., J. T. Devreese and F. M. Peeters, in *The Physics of the Two-Dimensional Electron Gas*, Vol. 157 of *NATO Advanced Study Institute, Series B: Physics*, edited by J. T. Devreese and F. M. Peeters (Plenum, New York, 1987), p. 131.

[14] X. Wu, F. M. Peeters, and J. T. Devreese, Phys. Rev. B **40**, 4090 (1989), and references cited therein.

[15] S. Das Sarma, Phys. Rev. B **27**, 2590 (1983); **31** 4034 (1985).

[16] D. M. Larsen, Phys. Rev. B **30**, 4595 (1984).

[17] M. Ziesmann, D. Heitmann, and L. L. Chang, Phys. Rev. B **35**, 4541 (1987).

[18] S. Pekar, Zh. Eksp. Teor. Fiz. **55**, 1997 (1968) [Sov. Phys. JETP **28**, 1054 (1969)]; S. I. Pekar, V. I. Sheka, and G. V. Dmitrenko, *ibid.* **63**, 1455 (1972) [Sov. Phys. JETP **36**, 771 (1973)].

[19] S. I. Pekar, L. S. Khazan, and V. I. Sheka, Zh. Eksp. Teor. Fiz. **65**, 1999 (1973) [Sov. Phys. JETP **38**, 999 (1974)].

[20] D. M. Larsen, J. Phys. C. **7**, 2877 (1974); **7**, 2890 (1974).

[21] H. Sigg, P. Wyder, and J. A. A. J. Perenboom, Phys. Rev. B **31**, 5253 (1985).

[22] K. Karrai, S. Huant, G. Martinez, and L. C. Brunel, Solid State Commun. **66**, 355 (1988).

[23] W. Seidenbusch, G. Lindemann, R. Lassnig, J. Edlinger, and E. Gornik, Surf. Sci. **142**, 375 (1984).

[24] U. Merkt, M. Horst, and J. P. Kotthaus, Phys. Scr. **T13**, 272 (1986).

[25] See Ref. 21.

[26] R. J. Nicholas, J. C. Portal, C. Houlbert, P. Perrier, and T. P. Pearsall, Appl. Phys. Lett. **34**, 492 (1993).

[27] J. Singleton, R. J. Nicholas, D. C. Roge, and C. T. B. Foxon, Surf. Sci. **196**, 429 (1988).

[28] C. M. Hu, T. Friedrich, E. Batke, K. Köhler, and P. Ganser, Phys. Rev. B **52**, 12 090 (1995).

[29] C. M. Hu, E. Batke, K. Köhler, and P. Ganser, Phys. Rev. Lett. **75**, 918 (1995); **76**, 1904 (1996).

[30] R. Lassnig and W. Zawadzki, Surf. Sci. **142**, 388 (1984).

[31] F. M. Peeters, X. G. Wu, J. T. Devreese, C. J. G. M. Langerak, J. Singleton, D. J. Barnes, and R. J. Nicholas, Phys. Rev. B **45**, 4296 (1992).
[32] F. M. Peeters, Wu Xiaoguang, and J. T. Devreese, Solid State Commun. **65**, 1505 (1988).
[33] G. Springholz and G. Bauer, Appl. Phys. Lett. **60**, 1660 (1992).
[34] G. Springholz, G. Bauer, and G. Ihninger, J. Cryst. Growth **127**, 302 (1993).
[35] S. Yuan, H. Krenn, G. Springholz, and G. Bauer, Phys. Rev. B **47**, 7213 (1993).
[36] S. Yuan, G. Springholz, G. Bauer, and H. Kriechbaum, Phys. Rev. B **49**, 5476 (1994).
[37] S. Yuan, H. Krenn, G. Springholz, G. Bauer, and H. Kriechbaum, Appl. Phys. Lett. **62**, 885 (1993).
[38] S. Yuan, G. Springholz, N. Frank, H. Krenn, G. Bauer, and M. Kriechbaum, in *Infrared Detectors—Materials, Processing, and Devices*, edited by L. R. Dawson and A. Appelbaum, MRS Symposia Proceedings No. 299 (Materials Research Society, Pittsburgh, 1994), p. 285.
[39] E. Koppensteiner, G. Springholz, P. Hamberger, and G. Bauer, J. Appl. Phys. **74**, 6062 (1993).
[40] G. Bauer, in *Landau Level Spectroscopy*, edited by G. Landwehr and E. I. Rashba (Elsevier, Amsterdam, 1991), p. 277.
[41] E. D. Palik and J. K. Furdyna, Rep. Prog. Phys. **33**, 1193 (1970).
[42] H. Burkhard, G. Bauer, and W. Zawadzki, Phys. Rev. B **19**, 5149 (1979).
[43] G. Bauer, H. Pascher, and W. Zawadzki, Semicond. Sci. Technol. **7**, 703 (1992), and references therein.
[44] P. G. Harper, Proc. Phys. Soc. **192**, 793 (1967).
[45] N. J. Johnson, H. Ehrenreich, P. M. Hui, and P. M. Young, Phys. Rev. B **41**, 3655 (1990).
[46] D. H. Dickey, E. J. Johnson, and D. M. Larsen, Phys. Rev. Lett. **18**, 599 (1967).
[47] P. Vogl and P. Kocevar, in *Proceedings of the International Conference on Physics of Semiconductors*, edited by B. L. H. Wilson, IOP Conf. Proc. No. 43 (Institute of Physics and Physical Society, London, 1978), p. 131.
[48] D. M. Larsen, Phys. Rev. B **36**, 3304 (1987).
[49] P. Pichler, G. Bauer, and H. Clemens, Z. Phys. B **67**, 475 (1987).
[50] C. J. G. M. Langerak, J. Singleton, P. J. van der Wel, J. A. A. Perenboom, D. J. Barnes, R. J. Nicholas, M. A. Hopkins, and C. T. B. Foxon, Phys. Rev. B **18**, 13 133 (1988).
[51] L. S. Kim, H. D. Drew, R. E. Doezema, J. P. Heremans, and D. L. Partin, Phys. Rev. B **35**, 2521 (1987).
[52] M. Kriechbaum, P. Kocevar, H. Pascher, and G. Bauer, IEEE J. Quantum Electron. **QE-24**, 1727 (1988).
[53] F. Geist, H. Pascher, G. Springholz, and G. Bauer, in *Proceedings of the International Conference on Narrow Gap Semiconductors*, edited by J. L. Reno, IOP Conf. Proc. No. 144 (Institute of Physics, Bristol, 1995), p. 145.
[54] D. L. Mitchell and R. F. Wallis, Phys. Rev. **151**, 581 (1965); see also: G. Bauer, in *Narrow Gap Semiconductors, Physics and Applications*, edited by W. Zawadzki, Springer Lecture Notes in Physics Vol. 133 (Springer, Berlin, 1980), p. 427.
[55] A. F. Terzis, X. C. Liu, A. Petrou, B. D. McCombe, M. Dutta, H. Shen, Doran D. Smith, M. W. Cole, M. Taysing-Lara, and P. G. Newman, J. Appl. Phys. **67**, 2501 (1990).
[56] G. Karczewski, J. K. Furdyna, D. L. Partin, C. N. Thrush, and J. P. Heremans, Phys. Rev. B **46**, 13 331 (1992).
[57] A. Krost, B. Harbecke, R. Faymonville, H. Schlegel, E. J. Fantner, K. E. Ambrosch, and G. Bauer, J. Phys. C **18**, 2119 (1985).
[58] H. Pascher, P. Röthlein, G. Bauer, and M. von Ortenberg, Phys. Rev. B **40**, 10 469 (1989).